8-16-2011

Estimating the Rayleigh-Wave Impulse Response Between Seismic Stations with the Cross Terms of the Green Tensor

Kasper van Wijk
Boise State University

T. Dylan Mikesell
Boise State University

Vera Schulte-Pelkum
University of Colorado at Boulder

Josh Stachnik
University of Colorado at Boulder

Estimating the Rayleigh-wave impulse response between seismic stations with the cross terms of the Green tensor

Kasper van Wijk,[1] T. Dylan Mikesell,[1] Vera Schulte-Pelkum,[2] and Josh Stachnik[2]

[1] The development of ambient noise tomography has provided a powerful tool to investigate the Earth's subsurface with increased resolution. Most commonly, surface-wave tomography is performed on inter-station estimates of the vertical component of Rayleigh waves, stemming from crosscorrelations of ocean-generated noise. Here, we estimate the cross terms of the Rayleigh-wave Green tensor, and show this is less sensitive to signal not in-line with the seismic stations. We illustrate this result with the Batholiths temporary seismic deployment, showing estimates of the Rayleigh wave with a higher signal-to-noise ratio and a consequently better phase-velocity dispersion curve. This approach provides an opportunity for reliable ambient noise crosscorrelations over shorter time windows and more closely spaced stations in the future. **Citation:** van Wijk, K., T. D. Mikesell, V. Schulte-Pelkum, and J. Stachnik (2011), Estimating the Rayleigh-wave impulse response between seismic stations with the cross terms of the Green tensor, *Geophys. Res. Lett.*, *38*, L16301, doi:10.1029/2011GL047442.

1. Introduction

[2] Being able to estimate the impulse response between seismic stations from crosscorrelating ambient noise has added a new dimension to surface-wave inversion for the Earth's lithosphere. Phase- and group-velocity dispersion curves between distributed station pairs are inverted for 3D velocity structure [e.g., *Sabra et al.*, 2005; *Shapiro et al.*, 2005; *Lin et al.*, 2008; *Ekström et al.*, 2009]. Ideally, station pairs are surrounded by noise sources so that the elastic Green tensor can be found by summing crosscorrelations of the different components (i, j) of the wavefield [*Wapenaar and Fokkema*, 2006, equation 87]:

$$G_{ij}(\mathbf{x}, \mathbf{x}', t) + G_{ij}(\mathbf{x}, \mathbf{x}', -t) \propto \oint_S u_i^S(\mathbf{x}, t) \star u_j^S(\mathbf{x}', t) d\mathbf{S}, \quad (1)$$

where $G_{ij}(\mathbf{x}, \mathbf{x}', t)$ is the Green tensor with component i at location $\mathbf{x}$ from a source in direction j at $\mathbf{x}'$. $u_i^S(\mathbf{x}, t) \star u_j^S(\mathbf{x}', t)$ denotes cross correlation of the components of the measured wavefield at $\mathbf{x}$ and $\mathbf{x}'$ from a source on contour S. In passive seismology, spatial integration is replaced with summation over k time sections of the wavefield u, aiming to capture surface-wave signal G_{ij}^R from ocean-generated noise around the stations at $(\mathbf{x}, \mathbf{x}')$:

$$G_{ij}^R(\mathbf{x}, \mathbf{x}', t) + G_{ij}^R(\mathbf{x}, \mathbf{x}', -t) \approx \sum_k \left(u_i(\mathbf{x}', t) \star u_j(\mathbf{x}, t) \right)_k. \quad (2)$$

[3] An uneven source distribution and contamination by wave modes other than Rayleigh waves can lead to artifacts in the estimated Green functions from crosscorrelation. *Wapenaar et al.* [2011] show in a numerical example how multi-dimensional deconvolution can suppress unwanted signal. While currently the vertical component $(i = j = z)$ of the Rayleigh wave is most commonly used in ambient noise tomography, we propose to estimate the cross terms of the Green tensor.

[4] A vertically heterogeneous earth has an anti-symmetry between the horizontal component of the Rayleigh wave from a vertical force source, and the vertical component of the Rayleigh wave from a horizontal force source [*Aki and Richards*, 2002, equation 7.147]:

$$G_{rz}^R(\mathbf{x}, \mathbf{x}', t) = -G_{rz}^R(\mathbf{x}', \mathbf{x}, t) = -G_{zr}^R(\mathbf{x}, \mathbf{x}', t), \quad (3)$$

where subscript r stands for radial and z for vertical. The first equality in this equation can be explained as follows: for a retrograde elliptical Rayleigh wave, G_{rz}^R is $\pi/2$ phase-delayed with respect to G_{zz}^R and π phase-delayed with respect to G_{zr}. The second equality is a result of reciprocity. Following equation (2), we compare G_{zz}^R to $G_{zr}^R - G_{rz}^R$. The Hilbert transform [e.g., *Claerbout*, 1985, p. 20] equalizes the phase between G_{zz} and the difference of the cross terms:

$$G_c^R(\mathbf{x}, \mathbf{x}', t) = \mathscr{H}\left[G_{zr}^R(\mathbf{x}, \mathbf{x}', t) - G_{rz}^R(\mathbf{x}, \mathbf{x}', t)\right]. \quad (4)$$

Crosscorrelations of multicomponent data from the Batholiths experiment [*Calkins et al.*, 2010] provide estimates of the cross terms of the Green tensor. We will show that G_c^R is more robust than G_{zz}^R in the presence of seismic signal not in-line with the seismic stations.

2. Batholiths Data

[5] Three-component measurements – at 40 samples per second – of the ambient noise wave field on stations of the Batholiths experiment serve to illustrate the robustness in estimating the cross terms of the Green function between seismic stations. The azimuth from station BN01 to BN23 from the north line of the Batholiths experiment is 29 degrees from North in the clockwise direction (Figure 1). We rotate the horizontal components of the wavefield recordings to a generally radial (r; parallel to 29 deg from N) and transverse (t; perpendicular to 29 deg from N) component, band-pass filter (0.1–1 Hz), and sign-bit the data. We crosscorrelate

[1]Department of Geosciences, Boise State University, Boise, Idaho, USA.
[2]CIRES and Department of Geological Sciences, University of Colorado at Boulder, Boulder, Colorado, USA.
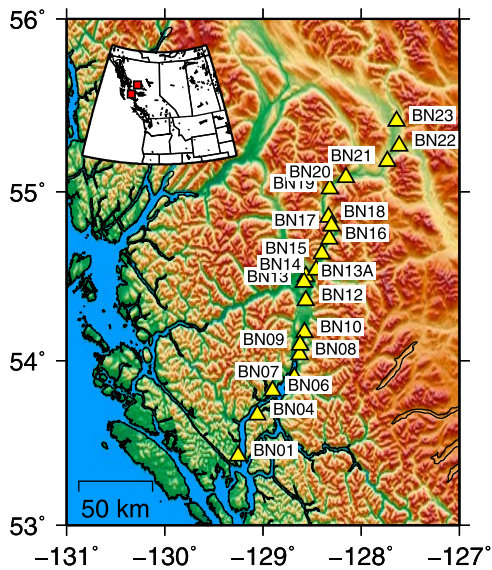
Figure 1. Location of the active stations in August of 2006 of the North line of the Batholiths experiment. Red squares on the regional inset are BN01 and BN23.

combinations of the vertical and radial components of the wavefield from station BN01 with those of all 20 active stations according to equation (2). The Green tensor estimate is the sum of non-overlapping, ten-minute cross-correlations from August 1, 2006 00:00:00 (HH:MM:SS) to August 4, 2006 00:00:00. We correct the amplitudes for geometrical spreading.

[6] We observe strong similarity in the Rayleigh-wave arrivals in Figure 2. However, G_{zz}^R contains coherent signal around $t = 0$ s for all stations, not present in G_c^R. This energy is the result of near-simultaneous arrivals on the vertical component at the stations $\mathbf{x}$ and $\mathbf{x}'$. The lack of this coherent noise in G_c^R means that u_r is less sensitive to it, which suggests the noise source is either surface-wave energy out of line with the seismic stations, or body-wave energy.
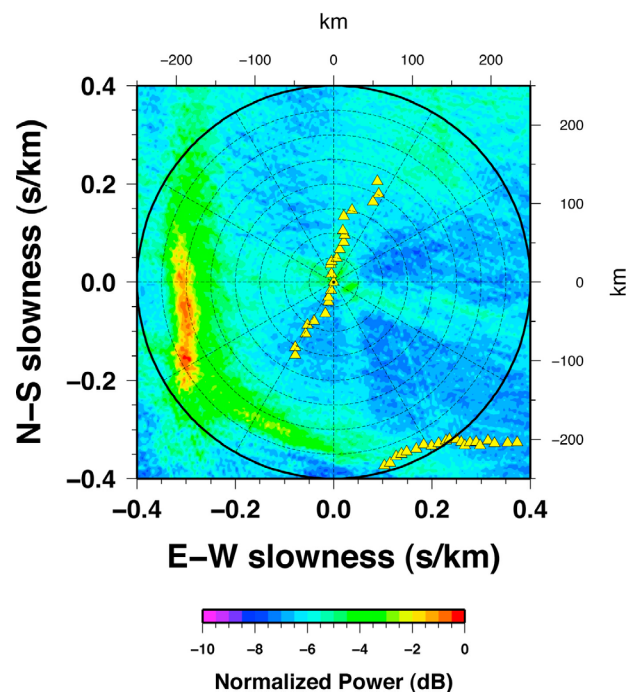
[7] To test for the presence of out-of-line surface- or body-wave energy inferred from the crosscorrelation results in Figure 2, we conduct a frequency-wavenumber (f-k) analysis [e.g., *Rost and Thomas*, 2002] of the vertical
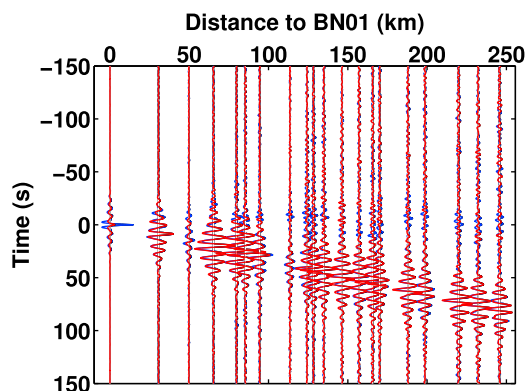
component records. We added the southern Batholiths station line, which has a close to E-W orientation (Figure 3), to increase resolution compared to beam forming with a linear array. The analysis is performed in the same frequency band as the crosscorrelations (0.1–1 Hz), using a 4th root beam [*Rost and Thomas*, 2002, equations 11 and 12] and taking the average of the absolute amplitudes in the beam window to calculate each value in the slowness grid. We apply the f-k analysis to consecutive one-hour segments spanning the same time window used in the crosscorrelations. All hourly slowness grids are stacked using the L1 norm, and the result normalized to the maximum amplitude in the grid. L-shaped arrays as used here smear energy in the direction of the array legs (see examples by *Rost and Thomas* [2002]). An array response function would show a cross shape of side lobes in slowness space matching the array geometry, with the maximum amplitude centered on the true incident slowness. This could explain the elongated shapes of the noise sources. Nevertheless, the southern source shown in Figure 3 is a true secondary source to the dominant western source, since the peak amplitude areas have large separation in slowness space and their amplitudes vary independently with time when viewed in the individual 1-hour f-k grids. Both source directions have slownesses typical for Rayleigh waves, with the dominant energy from the West propagating obliquely to the North station line used for the crosscorrelations. We identify this as the source for the out-of-line energy observed as the feature near $t = 0$ s in the vertical component crosscorrelations.

[8] For stations separated less than 175 km from BN01, the signal from out-of-line ocean noise interferes with the Rayleigh-wave arrival in G_{zz}^R. This can be observed in
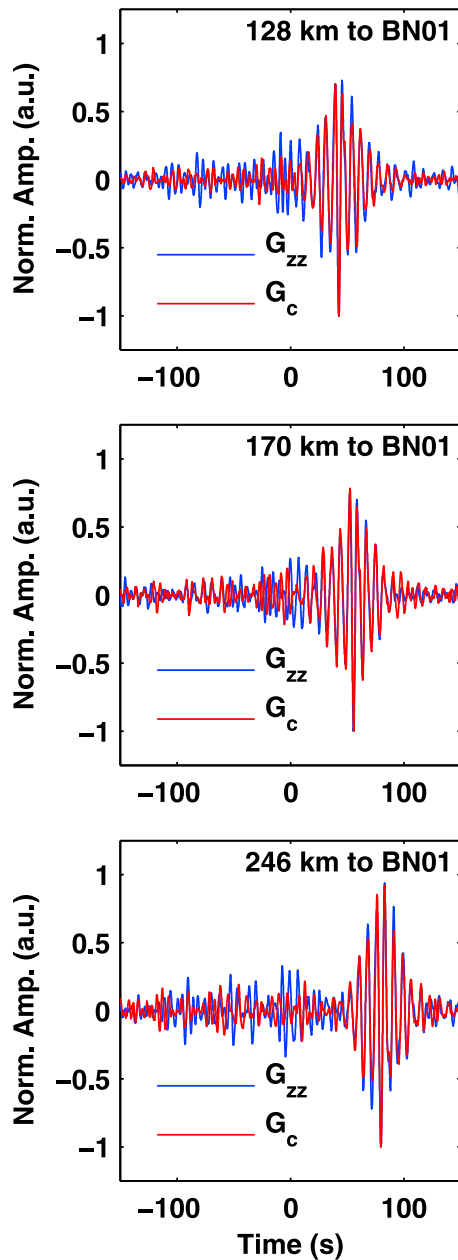

Figure 2. Estimated Green functions G_{zz}^R (blue) and G_c^R (red) from crosscorrelation of three days of ambient noise. For the smaller station spacings in G_{zz}^R, an artifact at $t \approx 0$ s interferes with the Rayleigh wave.

Figure 3. Summation of hourly f-k grids for the same three-day time window used in the crosscorrelations. Yellow triangles show station locations (distance scale on top and right). Dominant energy is from the West, with a secondary source of energy in the Southwest.

Figure 4. A comparison of the estimated Green functions for three stations. (top and middle) For the smaller two station spacings, noise at $t \approx 0$ s interferes with the Rayleigh-wave arrival in G_{zz}^R (blue), but this artifact is not present in G_c^R (red). (bottom) For wave fields with a large station spacings, noise and signal are separated in time.

[9] Next we use the five largest station spacings, where the Rayleigh wave arrival is distinctly later than the early-time noise, to quantify the improvement of using the cross terms by calculating the signal-to-noise ratio:

$$\text{SNR}_{dB} = 10 \log \left(\frac{A_{signal}}{A_{noise}} \right)^2, \qquad (5)$$

where A_{signal} and A_{noise} are the average amplitude in the time window of the Rayleigh wave ($35 < t < 100$ s) and of the noise ($t < 35$ s), respectively. For G_c^R, $\text{SNR}_{dB} = 14$ dB, compared to a much lower 5 dB for G_{zz}^R.

[10] To further illustrate the quality of G_c^R, we compute the phase-velocity dispersion curve – commonly used to invert for velocity structure – associated with G_c^R. We compute these phase-velocity dispersion curves using the Full-Offset Dispersion Imaging technique [*Park*, 2011], which includes spectral whitening in the phase-velocity transformation. Figure 5 contains automated picking of the maximum spectral energy from 0.1 to 0.29 Hz in the solid black lines. A direct comparison between these picks for the cross terms
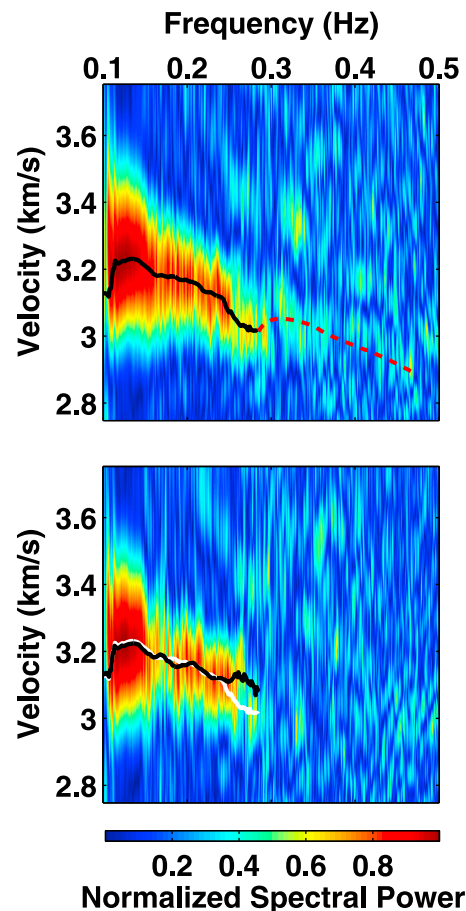
Figure 5. Phase velocity dispersion curve for the (top) esti-mated cross terms (G_c^R) and (bottom) vertical (G_{zz}^R) compo-nent of the Rayleigh wave. In Figure 5 (top), the black line is an automated pick, and the red dashed line is manual. In Figure 5 (bottom), we have no coherent energy above 0.29 Hz, and a comparison between the automated pick for G_{zz}^R (black) and G_c^R (white), shows significant differences particularly near 0.3 Hz.

Figure 2, and is highlighted by showing three of the waveforms in Figure 4. In Figures 4 (top) and 4 (middle) there is no clear time separation between the Rayleigh wave energy and the noise at early times. Only for large station separation – such as in Figure 4 (bottom) – can a time window separate signal from noise. This interference for the shorter station separations could lead to biased velocity and/or amplitude information in the estimate of the Rayleigh wave, which in turn could be erroneously attributed to attenuation and anisotropy (also discussed by *Harmon et al.* [2010]).

and the vertical component show significant differences, particularly from 0.25–0.29 Hz. In addition, we are able to manually pick the dispersion curve from 0.29–0.5 Hz for G_c^R, but not for G_{zz}^R. From 0.5–1 Hz we do not observe any more signal in either dispersion curve, which is consistent with what is known about the frequency content of ocean microseisms.

3. Conclusions

[11] Ambient-noise correlations of multicomponent wavefields from the Batholiths seismic experiment provide estimates of the Rayleigh-wave Green tensor. Taking advantage of the anti-symmetry of this tensor for laterally homogeneous media, the difference between the cross terms provides a superior estimate of the Rayleigh wave compared to the estimate from the vertical components. Beam forming shows that the improvement lies in the robustness of the cross terms in the presence of out-of-line Rayleigh-wave sources. The higher signal-to-noise ratio for the cross terms leads to superior dispersion information, and shows great promise to use smaller station spacings and shorter time averaging in the crosscorrelation process to achieve greater subsurface resolution.

[13] The Editor thanks the two anonymous reviewers for their assistance in evaluating this paper.

References

Aki, K., and P. G. Richards (2002), *Quantitative Seismology: Theory and Practice*, 2nd ed., Univ. Sci., Sausalito, Calif.

Calkins, J. A., G. Zandt, J. Girardi, K. Dueker, G. E. Gehrels, and M. N. Ducea (2010), Characterization of the crust of the Coast Mountains Batholith, British Columbia, from P to S converted seismic waves and petrologic modeling, *Earth Planet. Sci. Lett.*, *289*, 145–155.

Claerbout, J. F. (1985), *Fundamentals of Geophysical Data Processing*, Blackwell Sci., Palo Alto, Calif.

Ekström, G., G. A. Abers, and S. C. Webb (2009), Determination of surface-wave phase velocities across USArray from noise and Aki's spectral formulation, *Geophys. Res. Lett.*, *36*, L18301, doi:10.1029/2009GL039131.

Harmon, N., C. Rychert, and P. Gerstoft (2010), Distribution of noise sources for seismic interferometry, *Geophys. J. Int.*, *183*, 1470–1484.

Lin, F., M. P. Moschetti, and M. H. Ritzwoller (2008), Surface wave tomography of the western United States from ambient seismic noise: Rayleigh and Love wave phase velocity maps, *Geophys. J. Int.*, *173*, 281–298, doi:10.1111/j1365-1246X.2008.3720.x.

Park, C. B. (2011), Imaging dispersion of MASW data—Full vs. selective offset scheme, *J. Environ. Eng. Geophys.*, *16*, 13–23.

Rost, S., and C. Thomas (2002), Array seismology: Methods and applications, *Rev. Geophys.*, *40*(3), 1008, doi:10.1029/2000RG000100.

Sabra, K. G., P. Gerstoft, P. Roux, W. A. Kuperman, and M. C. Fehler (2005), Surface wave tomography from microseisms in Southern California, *Geophys. Res. Lett.*, *32*, L14311, doi:10.1029/2005GL023155.

Shapiro, N. M., M. Campillo, L. Stehly, and M. H. Ritzwoller (2005), High-resolution surface-wave tomography from ambient seismic noise, *Science*, *307*, 1615–1618.

Wapenaar, K., and J. Fokkema (2006), Green's function representations for seismic interferometry, *Geophysics*, *71*, SI33–SI46.

Wapenaar, K., E. Ruigrok, J. van der Neut, and D. Draganov (2011), Improved surface-wave retrieval from ambient seismic noise by multi-dimensional deconvolution, *Geophys. Res. Lett.*, *38*, L01313, doi:10.1029/2010GL045523.

Wessel, P., and W. H. F. Smith (1991), Free software helps map and display data, *Eos Trans. AGU*, *72*(41), 441.

T. D. Mikesell and K. van Wijk, Department of Geosciences, Boise State University, Boise, ID 83725, USA. (kaspervanwijk@boisestate.edu)

V. Schulte-Pelkum and J. Stachnik, CIRES, University of Colorado at Boulder, Boulder, CO 80309, USA.